J Mater Sci (2016) 51:2550–2557
DOI 10.1007/s10853-015-9567-y

Hollow Fe_3O_4@mesoporous carbon core–shell microspheres for efficient sorption of radionuclides

Shihao Xu[1] · Yingguo Zhao[1] · Fangcai Zheng[1] · Yuanguang Zhang[1]

Received: 20 July 2015 / Accepted: 4 November 2015 / Published online: 16 November 2015

Abstract Hollow Fe_3O_4@mesoporous carbon (h-Fe_3O_4@mC) microspheres have been synthesized using silica nanospheres as the sacrificial matrix. Physiochemical properties, surface morphology, and internal structures of the as-prepared products have been carefully characterized. The synthesized h-Fe_3O_4@mC microspheres have been applied to adsorb radionuclides from aqueous solutions and can be easily separated by an external magnetic field. Effects of contact time, pH, and initial concentrations on the interaction of h-Fe_3O_4@mC with U(VI), Eu(III), Co(II), and Sr(II) have been studied. The sorption is strongly dependent on pH and can reach equilibrium within 2 h. Dependence of sorption on pH is relevant to both the surface properties of sorbents and the relative distribution of radionuclides species in solutions. Due to the mesoporous structure, carboxyl-functionalized surface, and low density, h-Fe_3O_4@mC shows efficient sorption for radionuclides even in acidic solutions. The maximum sorption capacities of U(VI), Eu(III), Co(II), and Sr(II) on h-Fe_3O_4@mC at pH 3.0 and $T = 298$ K calculated from the Langmuir model are 0.566, 1.013, 0.860, and 0.733 mmol g^{-1}, respectively. Findings of the present work suggest that h-Fe_3O_4@mC can serve as a promising candidate for recovery and removal of radionuclides from aqueous solutions in the environmental pollution management.

✉ Yuanguang Zhang
aqyuanguangzhang@sina.com

[1] Anhui Collaborative Innovation Center for Petrochemical New Materials, Anqing Normal University, Anqing 246011, People's Republic of China

Introduction

As a mature technology capable of meeting the growing energy demands arising from fossil fuel depletion and increasing global population, nuclear power has also brought about a side effect: the nuclear waste. Radionuclides can pose a significant threat to human health and ecological systems because of their high toxicity, even at low concentrations. Therefore, safe treatment of aqueous waste effluents and contaminated groundwater containing human-made radionuclides has been an environmental concern to the public [1–4]. Several methods have been applied to remove radionuclides from contaminated water, such as precipitation [5], ion exchange [6], nanofiltration [7], electrosorption [8], biosorption [9], and sorption on solid substrates [10–12], among which sorption has been proven to be an effective and convenient technique for the separation and isolation of toxic species. Sorption of radionuclides by natural minerals such as sepiolite and attapulgite has been extensively investigated but the limited sorption capacity hinders their practical applications. Thus, novel sorbents which are inexpensive, effective, and environmentally friendly need to be developed for the remediation of radionuclides from aqueous solutions.

During the last decade, interest in the use of new carbon materials for environmental applications has increased significantly [13–15]. As a new member of the carbonaceous material family, ordered mesoporous carbon has attracted considerable attention because of its high surface area, regular mesopore, large pore volume, as well as excellent chemical and physical stability. Its high sorption capacity and fast sorption rate make it a promising new material for the removal of a large variety of pollutants such as dyes and heavy metals [16–19]. Most surfaces of mesoporous carbon are hydrophobic which makes its

sorption of positively charged metal ions in aqueous solutions inefficient. Functionalization of the carbon surface is achieved mainly via multistep post-synthesis oxidation methods which are time and resource consuming. Recent researches have demonstrated that carboxyl and negative charge-functionalized mesoporous carbon can be synthesized conveniently using ferrocene as a single reactant [20, 21]. However, systematic study on the application of mesoporous carbon in sorption of radionuclides has not been widely reported. Therefore, it would be interesting to explore the possibility of preparing a noval sorbent based on the carboxyl-functionalized mesoporous carbon for recovery of radionuclides from aqueous solutions.

Convenient separation of sorbents from aqueous phase is of special importance considering the recyclability of sorbents and the recoverability of sorbates that are either toxic or precious. Compared to traditional separation methods such as centrifugation and filtration which are labor-consumptive and uneconomical, magnetic separation is a practical and effective means for large-scale water treatment [22–25]. There are many efforts to combine in a single solid the convenience of magnetic separation with the high sorption capacity of mesoporous carbon, most of which focus on the magnetite/mesoporous carbon core–shell composite. The carbon shell can protect the magnetite core in oxidative and acidic environments and improve the dispersibility of the colloidal suspensions in aqueous solutions. However, the solid cores without any recognition sites possess most mass of the core–shell composite (about 80 %), which correspondingly decrease the sorption capacity per unit mass [26, 27]. Hollow particles with a single hole in the core show advantages over the same-sized solid particles due to lower density and higher specific surface area.

In this context, monodispersed hollow Fe_3O_4@mesoporous carbon (h-Fe_3O_4@mC) microspheres were synthesized using silica nanospheres as the sacrificial matrix. The synthesized materials were carefully characterized and used to adsorb radionuclides [U(VI), Eu(III), Sr(II), and Co(II)] from aqueous solutions. These radionuclides are chosen in order to investigate the influence of chemical valence, ionic valence, and ionic size on the sorption process. The kinetics of sorption, pH sorption edges, and sorption capacity were studied in the batch sorption mode to illustrate the performance of h-Fe_3O_4@mC in recovering radionuclides from aqueous solutions.

Experimental section

Materials

Absolute ethyl alcohol, ammonia water (25 %), tetraethyl silicate (TEOS, 98 %), ferrocene (98 %), acetone (99 %), and hydrogen peroxide (30 %) were purchased from Sinopharm Chemical Reagent Co., Ltd. All chemicals were of analytical purity and used without further purification.

Preparation of SiO_2@Fe_3O_4@mesoporous carbon

First, monodispersed SiO_2 nanospheres with the diameter of about 100 nm were synthesized according to the Stöber method [28]. Briefly, 20 ml of ethanol, 10 ml of distilled water, and 4.0 ml of ammonia water were mixed to obtain a homogeneous solution with the help of ultrasonication. Then 1.0 ml of TEOS was added to the mixture dropwise. After 4 h of reaction under stirring, the nanoparticles of SiO_2 were obtained and washed with ethanol and distilled water several times.

Afterwards, 25 mg of SiO_2 synthesized above and 100 mg of ferrocene were dispersed in 30 ml of acetone. After 10 min of intense sonication and 5 min of stirring, 1.0 ml of hydrogen peroxide was added into the mixture dropwise. The mixture was then stirred vigorously for 3 h and transferred to the Teflon-lined stainless-steel autoclave (50 ml capacity). The autoclave was heated to and maintained at 200 °C for 48 h, and then allowed to cool to room temperature. The obtained product was collected by using a magnet, washed with ethanol and distilled water alternatively, and denoted as SiO_2@Fe_3O_4@mC.

Preparation of hollow Fe_3O_4@mesoporous carbon

The as-prepared SiO_2@Fe_3O_4@mC nanoparticles were redispersed in 30 ml of distilled water. Then 3.0 ml of ammonia water was added to the mixture under stirring. After several minutes of intense ultrasonication, the mixture was transferred to a Teflon-lined stainless-steel autoclave with volume of 50 ml and heated to and maintained at 150 °C for 12 h. After been cooled to room temperature, the product was washed with ethanol and distilled water several times and denoted as h-Fe_3O_4@mC.

Characterization

X-ray diffraction (XRD) patterns of materials were obtained on a Philips X'Pert Pro Super X-ray diffractometer using Cu-K_α radiation. The nitrogen adsorption and desorption isotherms at −196 °C were measured using a TriStar 3000 volumetric adsorption analyzer (Micromeritics Instrument Corp., Norcross, GA). The samples were pretreated at 200 °C overnight under vacuum. Fourier transformed infrared (FTIR) spectra were obtained on a Nicolet Magna-IR 750 spectrometer with KBr pellets at room temperature. Scanning electron microscopic (SEM) images were recorded by using a JEOL JSM-6330F microscope. Transmission electron microscopic (TEM)

images were obtained on a JEOL-2010 microscope. Magnetic measurements were carried out in a MPMS-XL SQUID magnetometer. Surface charge was measured using Particles Analyzer (Delsa Nano C, Beckman Coulter).

Sorption experiments

The sorption performance was investigated by the batch method. Stock solutions of sorbents and $NaClO_4$ solutions were pre-equilibrated for 24 h followed by the addition of radionuclides stock solution to achieve specific concentrations of different compositions. Negligible amounts of $HClO_4$ and/or NaOH solutions were added to adjust the pH to desired values. After being shaken for 12 h to achieve sorption equilibration, the solid phase was separated from the suspension using a permanent magnet, and the concentrations of radionuclides in the supernatants were measured by inductively coupled plasma atomic emission spectroscopy (ICP-AES, Thermo Elemental, USA). The sorption percentage and amounts of radionuclides adsorbed on the solid phase (q_e) were calculated as follows:

$$\text{Sorption } (\%) = \frac{C_0 - C_e}{C_0} \times 100\,\% \quad (1)$$

$$q_e = \frac{(C_0 - C_e) \times V}{m}, \quad (2)$$

where C_0 and C_e correspond to the initial and equilibrium concentrations of radionuclides, V is the volume of the suspension, and m is the mass of the dry sorbent.

Results and discussion

Characterization

Figure 1 is the XRD pattern of h-Fe_3O_4@mC. The six main diffraction peaks indexed to (220), (311), (400), (422), (511), and (440) indicate the existence of Fe_3O_4 with a face-centered cubic structure. No peaks from carbon are observed due to the strong signals of iron oxides which can overwhelm the weak carbon peaks. The magnetization curve of h-Fe_3O_4@mC measured at room temperature is shown in Fig. 2. The saturation magnetization is 65.5 emu g^{-1}, which guarantees the high efficiency of magnetic separation.

In order to identify the composition and functional groups of the as-prepared nanoparticles, FTIR spectra of SiO_2@Fe_3O_4@mC and h-Fe_3O_4@mC are shown in Fig. 3. The peak at 587 cm^{-1} is attributed to the stretching vibration of the Fe–O bond. The absorption bands around 1600 and 3400 cm^{-1} indicate the existence of carboxyl functional groups. The broad band around 1100 cm^{-1} is attributed to Si–O–Si and Si–O–H stretching vibrations, and the peak at 466 cm^{-1} corresponds to the bending vibration of O–Si–O [29]. After etching by ammonia water, the characteristic absorption bands of silica for h-Fe_3O_4@mC disappear in Fig. 3, indicating that silica has been successfully removed.

Surface morphology and internal features can be observed by SEM and TEM. Figure 4a is the SEM image of the as-prepared SiO_2. It shows that the product consists of a large quantity of monodispersed spheres with an average diameter of about 100 nm. Figure 4b, c are the SEM images of SiO_2@Fe_3O_4@mC and h-Fe_3O_4@mC, respectively. Both SiO_2@Fe_3O_4@mC and h-Fe_3O_4@mC feature a clear spherical shape and have a uniform size of about 130 nm, which is about 30 nm bigger than that of

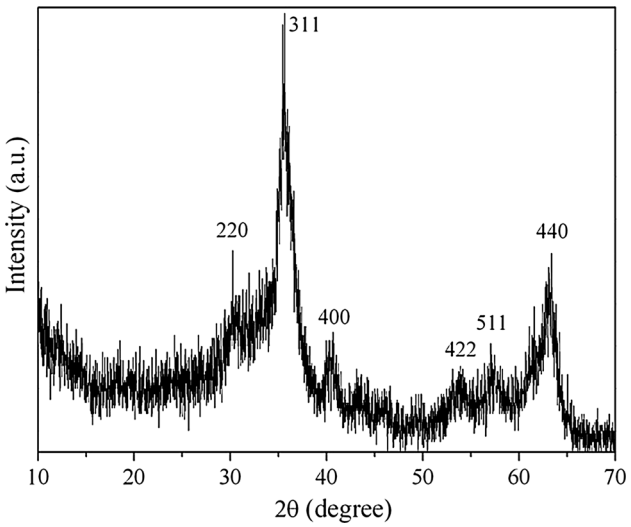

Fig. 1 XRD pattern of h-Fe_3O_4@mC

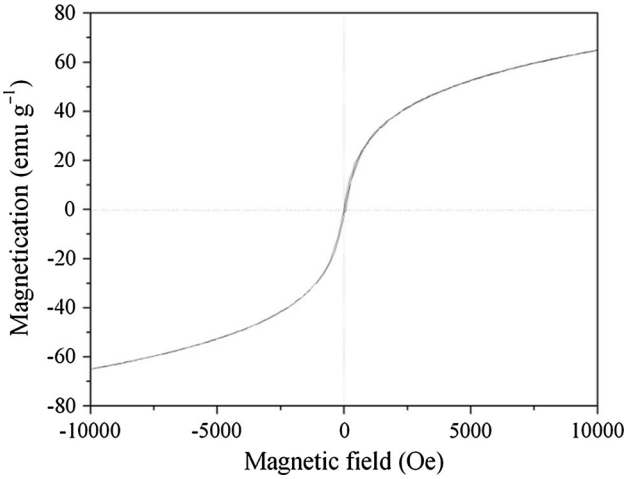

Fig. 2 Magnetization curve of h-Fe_3O_4@mC

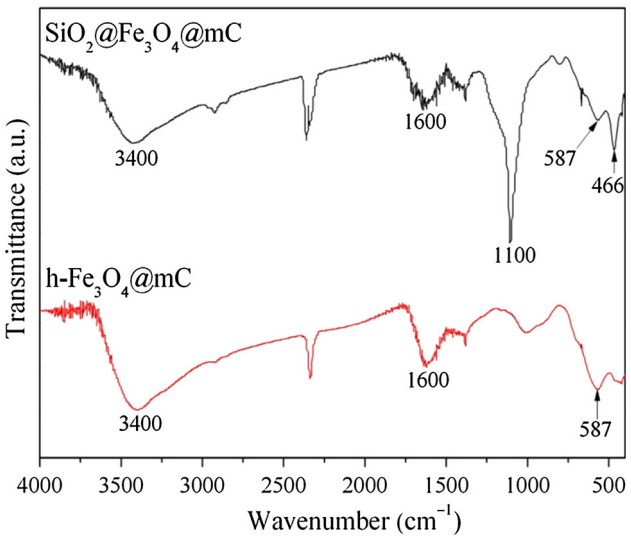

Fig. 3 FTIR spectra of SiO_2@Fe_3O_4@mC and h-Fe_3O_4@mC

pure silica due to the coating of double shells (Fe_3O_4 and mesoporous carbon). Figure 4b, c also indicates that the surface of h-Fe_3O_4@mC is much rougher than that of SiO_2@Fe_3O_4@mC, which can be attributed to etching of the carbon layer by ammonia water under hydrothermal conditions. This etching process is also expected to increase the surface area of the nanoparticles and thus enhance the loading capacities of radionuclides. The TEM image of SiO_2@Fe_3O_4@mC (Fig. 4d) clearly demonstrates the double-shelled structure with the inner silica core, the middle magnetite layer, and the outer mesoporous carbon layer. After etching by ammonia water, a cavity with a diameter of about 100 nm in the center of the nanoparticles can be observed in the TEM images of h-Fe_3O_4@mC (Fig. 4e, f), which is in accordance with the size of the silica template.

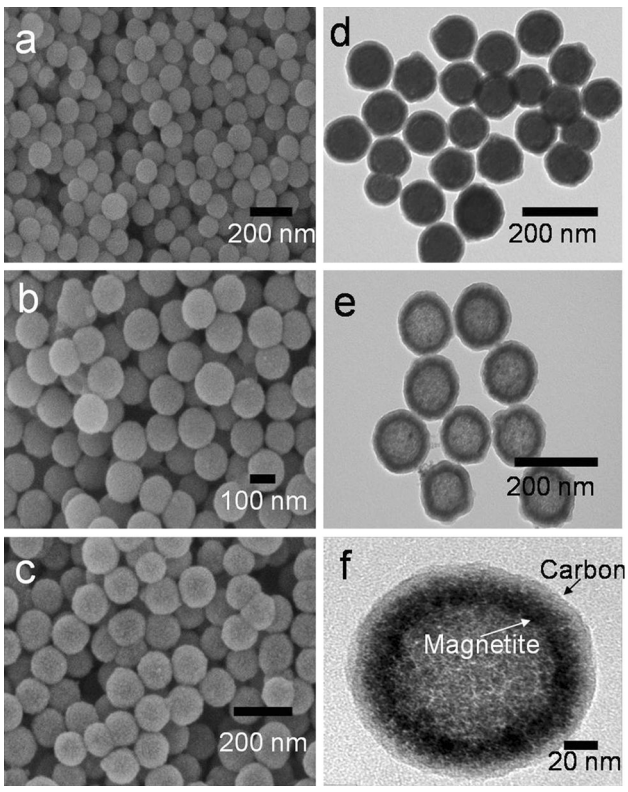

Fig. 4 SEM images of SiO_2 (**a**), SiO_2@Fe_3O_4@mC (**b**), and h-Fe_3O_4@mC (**c**); TEM images of SiO_2@Fe_3O_4@mC (**d**) and h-Fe_3O_4@mC (**e**), and HRTEM image of h-Fe_3O_4@mC (**f**)

The porous properties of nanoparticles can be investigated by using N_2 adsorption–desorption isotherms. As shown in Fig. 5, the adsorption–desorption isotherms of h-Fe_3O_4@mC exhibit type-IV curves according to the IUPAC classification, which is typical for mesoporous materials. The pore size distribution curve (the inset of Fig. 5) calculated using the Barrett–Joyner–Halenda (BJH) model from the adsorption branch demonstrates a sharp peak centered at 5.2 nm, indicating the uniform mesoporous structure. The surface area is calculated to be 83.1 $m^2\ g^{-1}$ through the Brunauer–Emmett–Teller (BET) method, and the total pore volume is calculated to be 0.27 $cm^3\ g^{-1}$ from the adsorption amount at a relative pressure of 0.998. The uniform porous structure, large surface area, and total pore volume could be responsible for their high sorption capacities.

Time-dependent sorption

The sorption rate is an important factor while evaluating the overall performance of sorbents. The dependence of radionuclide removal on contact time is presented in Fig. 6. For all radionuclides investigated, the sorption rates

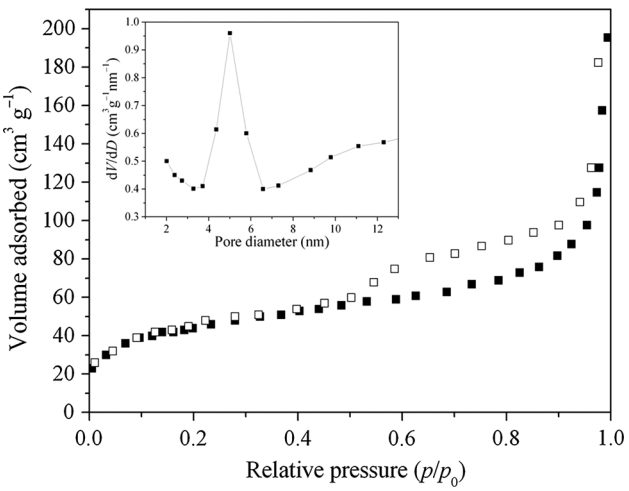

Fig. 5 Nitrogen adsorption–desorption isotherms for h-Fe_3O_4@mC. The *inset* shows the pore size distribution

increase quickly in the first hour of contact time and then slow down with increasing contact time. The initial rapid sorption can be attributed to the existence of plentiful binding sites. As contact time increases, there are less free binding sites available on the sorbents, approaching to steady states at the later stages [30, 31]. The short time needed to reach sorption equilibrium indicates that h-Fe_3O_4@mC may have good application potentials in remediation of radionuclides from large volumes of aqueous solutions. Based on the kinetic data, 12 h was selected to guarantee fully sorption equilibrium in the following experiments.

Effects of pH on sorption

Solution pH has a great impact on radionuclide sorption [32–34]. Figure 7 shows pH sorption edges for U(VI), Eu(III), Co(II), and Sr(II). For Sr(II), sorption increases gradually in the whole pH range involved in this study. For Eu(III) and Co(II), sorption increases as pH increases at low pH and then remain steady at high pH. The sorption amount of U(VI) increases gradually when pH increases from 2.0 to 6.0 and then falls off at pH values higher than 8.0.

The different trends of pH-dependent sorption can be attributed to the influence of pH on both the surface properties of sorbents and the relative distribution of radionuclide species in solutions. The zeta potentials of the as-obtained products at different pH are shown in Fig. 8, which indicates that the surface of the particles is positively charged at pH <2.3 and is negatively charged at pH >2.3. Figure 9 shows the distribution of radionuclide species in aqueous solutions. For Sr(II), in the whole pH range, the main species are positively charged cations Sr^{2+} and no precipitation forms. Therefore, the sorption of Sr(II) on the

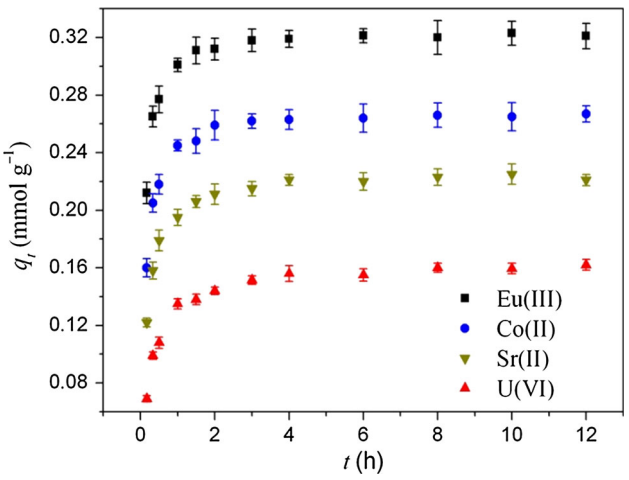

Fig. 6 Sorption of radionuclides on h-Fe_3O_4@mC as a function of contact time. pH 3.0, $T = 298$ K, $I = 0.01$ mol L^{-1} $NaClO_4$, $C_{initial} = 0.2$ mmol L^{-1}, and $m/V = 0.2$ g L^{-1}

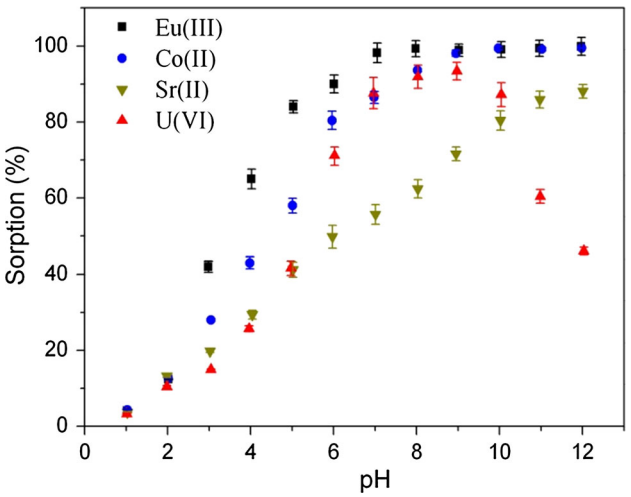

Fig. 7 Effect of pH on radionuclide sorption on h-Fe_3O_4@mC. $T = 298$ K, $I = 0.01$ mol L^{-1} $NaClO_4$, $C_{initial} = 0.2$ mmol L^{-1}, and $m/V = 0.2$ g L^{-1}

composites increases gradually due to the electrostatic attraction between the positive charge of cations and the increasing negative charge of sorbents. For Eu(III) and Co(II), precipitation can be witnessed at high pH, and thus, the sorption amount maintains a high level. The negative effect of increasing pH on U(VI) sorption at pH >7.0 could be attributed to the electrostatic repulsion of uranium anions such as $UO_2(OH)_3^-$ and $UO_3(OH)_7^-$ with the negatively charged surfaces of h-Fe_3O_4@mC, and possible formation of soluble carbonate complexes.

Sorption isotherms

Sorption isotherms depict the dependence of sorption amounts on the initial radionuclide concentrations and are shown in Fig. 10. Considering the generally low solution

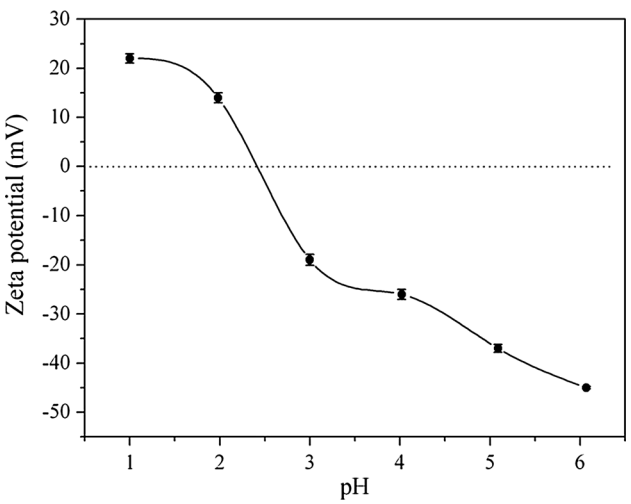

Fig. 8 Zeta potentials of h-Fe_3O_4@mC in solutions with different pH values

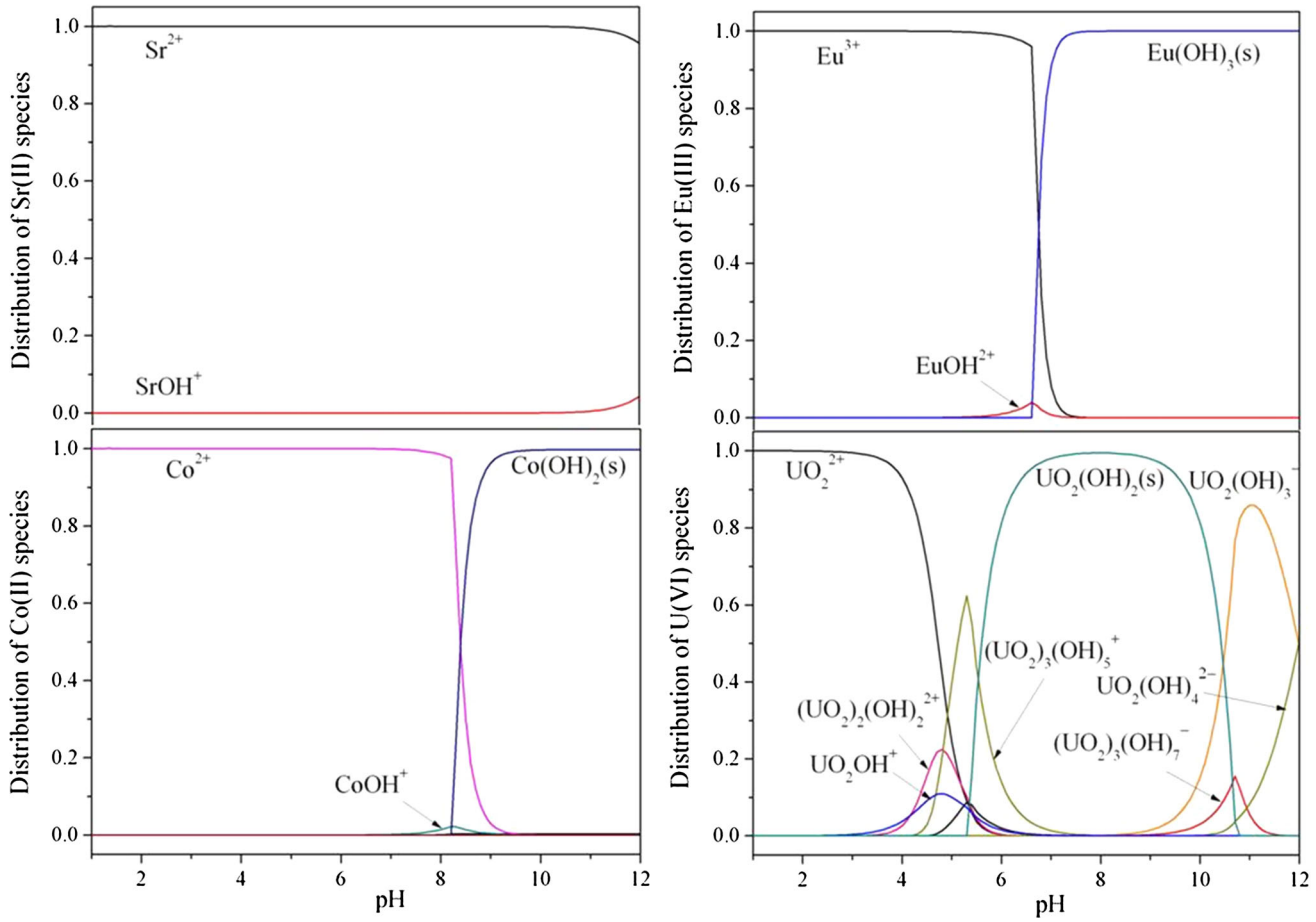

Fig. 9 Distribution of radionuclide species in 0.01 mol L^{-1} $NaClO_4$ calculated using Visual MINTEQ version 3.0. $T = 298$ K and $C_{initial} = 0.2$ mmol L^{-1}

pH of nuclear wastewater and possible formation of precipitation of radionuclides at high pH, all the sorption isotherms were obtained at pH of 3.0.

The differences in sorption capacities of sorbents for different radionuclides can be attributed to differences in ionic valence and ionic size. The surface of h-Fe_3O_4@mC is negatively charged at pH of 3.0; therefore, more positively charged species are expected to bind with sorbents more easily. However, the sorption capacity is not directly relevant to the chemical valence of radionuclides. For example, U(VI) is hexavalent and Eu(III) is trivalent, but sorption of Eu(III) is higher than that of U(VI). The main reason can be found from the species distribution curves in Fig. 9. Although U(VI) is hexavalent, the main species of U(VI) at pH 3.0 is the divalent UO_2^{2+} cation. On the contrary, the main species of Eu(III) in this case is the trivalent Eu^{3+} cation. Ions with higher positive valence are expected to exhibit stronger electrostatic affinity to the negatively charged surfaces of sorbents and thus have higher sorption capacities. For equivalent ions, binding

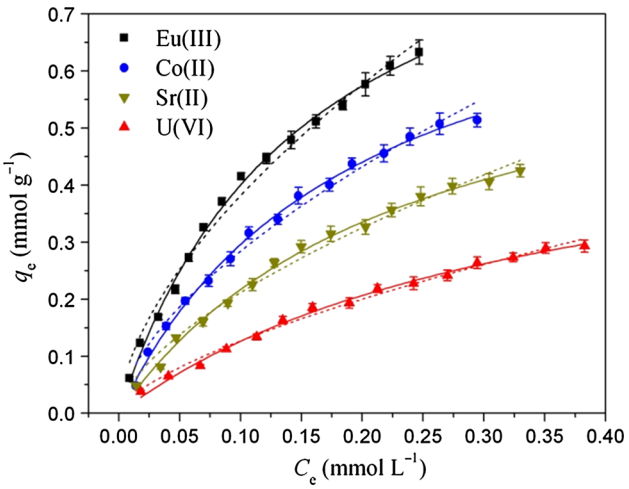

Fig. 10 Sorption isotherms of radionuclide sorption on h-Fe_3O_4@mC. pH 3.0, $T = 298$ K, $I = 0.01$ mol L^{-1} $NaClO_4$, and $m/V = 0.2$ g L^{-1}. The scattered points represent experiment data, the *solid lines* represent the Langmuir model, and the *dashed lines* represent the Freundlich model

Table 1 Parameters for the Langmuir and Freundlich models of radionuclide sorption on h-Fe_3O_4@mC

Sorbates	Langmuir			Freundlich		
	q_{max} (mmol g^{-1})	b (L $mmol^{-1}$)	R^2	k_F ($mmol^{1-n}$ L^n g^{-1})	n	R^2
Eu(III)	1.013	6.530	0.996	1.502	1.681	0.987
Co(II)	0.860	5.246	0.997	1.145	1.653	0.986
Sr(II)	0.733	4.204	0.996	0.881	1.616	0.986
U(VI)	0.566	2.874	0.994	0.575	1.524	0.990

performance is mainly affected by ionic size. According to previous studies, the ionic radius of Co^{2+} is smaller than that of Sr^{2+}, and the linear shaped UO_2^{2+} has the biggest length [35]. Smaller ions adsorbed occupy smaller surface area of sorbents, thus leading to higher sorption amounts. Therefore, sorption amounts of these radionuclides is in the order Eu(III) > Co(II) > Sr(II) > U(VI).

The sorption isotherms are fitted by Langmuir and Freundlich models, respectively:

$$q_e = \frac{bq_{max}C_e}{1 + bC_e} \quad (3)$$

$$q_e = k_F C_e^{1/n}, \quad (4)$$

where q_e and C_e are concentrations of radionuclides in equilibrium solid phase (mmol g^{-1}) and liquid phase (mmol L^{-1}), respectively; b (L $mmol^{-1}$) is the Langmuir sorption coefficient; q_{max} (mmol g^{-1}) is the maximum sorption capacity; k_F ($mmol^{1-n}$ L^n g^{-1}) is the Freundlich sorption coefficient; and n is an indicator of isotherm nonlinearity. Values of parameters for the Langmuir and Freundlich models are presented in Table 1. Based on the correlation coefficients (R^2) and the fitting curves in Fig. 10, the experimental data are fitted better by the Langmuir model than by the Freundlich model, indicating the monolayer sorption process and the binding interactions between radionuclides and h-Fe_3O_4@mC.

Conclusions

Radionuclides can pose a significant threat to human health and ecological systems, and safe treatment of aqueous waste effluents and contaminated groundwater containing human-made radionuclides has been an environmental concern to the public. Herein, hollow Fe_3O_4@mesoporous carbon (h-Fe_3O_4@mC) microspheres have been successfully synthesized, carefully characterized, used to adsorb radionuclides from aqueous solutions, and can be easily collected by an external magnetic field. The influence of pH on sorption is strongly dependent on both the surface properties of sorbents and the relative distribution of radionuclide species in solutions. The hollow cavity decreases the density, the mesopore affords huge active sites, and the carboxyl functionalization enhances affinity toward positively charged ions of radionuclides, all of which are beneficial to the sorption performance. Sorption processes of U(VI), Eu(III), Co(II), and Sr(II) on h-Fe_3O_4@mC reach equilibrium in 2 h of contact time and the maximum sorption capacities are 0.566, 1.013, 0.860, and 0.733 mmol g^{-1}, respectively. High sorption capacity and fast sorption rate make h-Fe_3O_4@mC a promising material for radionuclide containment and removal.

Acknowledgements The authors acknowledge the financial support from the National Natural Science Foundation of China (21371009).

References

1. Manos MJ, Kanatzidis MG (2012) Layered Metal Sulfides Capture Uranium from Seawater. J Am Chem Soc 134:16441–16446
2. Fan Q, Li P, Chen Y, Wu W (2011) Preparation and application of attapulgite/iron oxide magnetic composites for the removal of U(VI) from aqueous solution. J Hazard Mater 192:1851–1859
3. Li J, Guo Z, Zhang S, Wang X (2011) Enrich and seal radionuclides in magnetic agarose microspheres. Chem Eng J 172:892–897
4. Scott TB, Allen GC, Heard PJ, Randell MG (2005) Reduction of U(VI) to U(IV) on the surface of magnetite. Geochim Cosmochim Acta 69:5639–5646
5. Kanematsu M, Perdrial N, Um W, Chorover J, O'Day PA (2014) Influence of phosphate and silica on U(VI) precipitation from acidic and neutralized wastewaters. Environ Sci Technol 48:6097–6106
6. Ye M, Lu Z, Hu Y, Zhang Q, Yin Y (2013) Mesoporous titanate-based cation exchanger for efficient removal of metal cations. J Mater Chem A 1:5097–5104
7. Reff O, Wilken RD (1999) Removal of dissolved uranium by nanofiltration. Desalination 122:147–150
8. Jung CH, Lee HY, Moon JK, Won HJ, Shul YG (2011) Electrosorption of uranium ions on activated carbon fibers. J Radioanal Nucl Chem 287:833–839
9. Das N (2012) Remediation of radionuclide pollutants through biosorption-an overview. Clean-Soil Air Water 40:16–23
10. Awual MR, Yaita T, Taguchi T, Shiwaku H, Suzuki S, Okamoto Y (2014) Selective cesium removal from radioactive liquid waste by crown ether immobilized new class conjugate adsorbent. J Hazard Mater 278:227–235
11. Wang X, Pei Y, Lu M, Lu X, Du X (2015) Highly efficient adsorption of heavy metals from wastewaters by graphene oxide-ordered mesoporous silica materials. J Mater Sci 50:2113–2121. doi:10.1007/s10853-014-8773-3

12. Awual MR, Suzuki S, Taguchi T, Shiwaku H, Okamoto Y, Yaita T (2014) Radioactive cesium removal from nuclear wastewater by novel inorganic and conjugate adsorbents. Chem Eng J 242:127–135
13. Sun Y, Shao D, Chen C, Yang S, Wang X (2013) Highly efficient enrichment of radionuclides on graphene oxide-supported polyaniline. Environ Sci Technol 47:9904–9910
14. Chen H, Shao D, Li J, Wang X (2014) The uptake of radionuclides from aqueous solution by poly(amidoxime) modified reduced graphene oxide. Chem Eng J 254:623–634
15. Romanchuk AY, Slesarev AS, Kalmykov SN, Kosynkin DV, Tour JM (2013) Graphene oxide for effective radionuclide removal. PCCP 15:2321–2327
16. Li Z, Ren S (2015) Preparation of nitrogen-functionalized mesoporous carbon and its application for removal of copper ions. J Mater Sci 50:4600–4609. doi:10.1007/s10853-015-9009-x
17. Zhang Z, Zhou Y, Liu Y, Cao X, Zhou Z, Han B, Liang P, Xiong G (2014) Removal of thorium from aqueous solution by ordered mesoporous carbon CMK-3. J Radioanal Nucl Chem 302:9–16
18. Liu Y, Zeng G, Tang L, Cai Y, Pang Y, Zhang V, Yang G, Zhou Y, He X, He Y (2015) Highly effective adsorption of cationic and anionic dyes on magnetic Fe/Ni nanoparticles doped bimodal mesoporous carbon. J Colloid Interface Sci 448:451–459
19. Baikousi M, Georgiou Y, Daikopoulos C, Bourlinos AB, Filip J, Zboril R, Deligiannakis Y, Karakassides M (2015) Synthesis and characterization of robust zero valent iron/mesoporous carbon composites and their applications in arsenic removal. Carbon 93:636–647
20. Wang H, Chen Q, Chen J, Yu B, Hu X (2011) Carboxyl and negative charge-functionalized superparamagnetic nanochains with amorphous carbon shell and magnetic core: synthesis and their application in removal of heavy metal ions. Nanoscale 3:4600–4603
21. Wang H, Sun Y, Yu Y, Chen J, Li R, Cheng K, Chen Q (2012) A general route to synthesize water-dispersive noble metal-iron oxide bifunctional hybrid nanoparticles. Dalton Trans 41:346–350
22. Chandra V, Park J, Chun Y, Lee JW, Hwang IC, Kim KS (2010) Water-dispersible magnetite–reduced graphene oxide composites for arsenic removal. ACS Nano 4:3979–3986
23. Akin I, Arslan G, Tor A, Ersoz M, Cengeloglu Y (2012) Arsenic(V) removal from underground water by magnetic nanoparticles synthesized from waste red mud. J Hazard Mater 235:62–68
24. Koo HY, Lee HJ, Go HA, Lee YB, Bae TS, Kim JK, Choi WS (2011) Graphene-based multifunctional iron oxide nanosheets with tunable properties. Chem Eur J 17:1214–1219
25. Zhao Y, Li J, Zhao L, Zhang S, Huang Y, Wu X, Wang X (2014) Synthesis of amidoxime-functionalized Fe_3O_4@SiO_2 core-shell magnetic microspheres for highly efficient sorption of U(VI). Chem Eng J 235:275–283
26. Xie L, Guo J, Zhang Y, Hu Y, You Q, Shi S (2015) Novel molecular imprinted polymers over magnetic mesoporous silica microspheres for selective and effi-cient determination of protocatechuic acid in Syzygium aromatium. Food Chem 178:18–25
27. Xie L, Guo J, Zhang Y, Shi S (2014) Efficient determination of protocatechuicacid in fruit juices by selective and rapid magnetic molecular imprinted solidphase extraction coupled with HPLC. J Agric Food Chem 62:8221–8228
28. Stober W, Fink A, Bohn E (1968) Controlled growth of monodisperse silica spheres in the micron size range. J Colloid Interface Sci 26:62–69
29. Sadeghi S, Azhdari H, Arabi H, Moghaddam AZ (2012) Surface modified magnetic Fe_3O_4 nanoparticles as a selective sorbent for solid phase extraction of uranyl ions from water samples. J Hazard Mater 215:208–216
30. Ho YS, McKay G (2000) The kinetics of sorption of divalent metal ions onto sphagnum moss peat. Water Res 34:735–742
31. Ho YS (2006) Review of second-order models for adsorption systems. J Hazard Mater 136:681–689
32. Joseph C, Stockmann M, Schmeide K, Sachs S, Brendler V, Bernhard G (2013) Sorption of U(VI) onto opalinus clay: effects of pH and humic acid. Appl Geochem 36:104–107
33. Ilton ES, Wang ZM, Boily JF, Qafoku O, Rosso KM, Smith SC (2012) The effect of pH and time on the extractability and speciation of uranium(VI) sorbed to SiO_2. Environ Sci Technol 46:6604–6611
34. Camacho LM, Deng SG, Parra RR (2010) Uranium removal from groundwater by natural clinoptilolite zeolite: effects of pH and initial feed concentration. J Hazard Mater 175:393–398
35. Song W, Wang X, Wang Q, Shao D, Wang X (2015) Plasma-induced grafting of polyacrylamide on graphene oxide nanosheets for simultaneous removal of radionuclides. PCCP 17:398–406